PARAROTORS FOR PLANETARY ATMOSPHERE EXPLORATION

V. Nadal-Mora [(1)], J. Piechoki [(2)], A. Cuerva, [(3)], A. Sanz-Andres[(4)], S. Franchini[(5)],

[(1)] Professor (a), *Email:* vnadal@ing.unlp.edu.ar
[(2)] Doctorat student (a), *Email:* joaquinpiechocki@gmail.com
[(3)] Professor (b), *Email:* alvaro.cuerva@upm.es
[(4)] Full Professor (b), *Email:* angel.sanz.andres@upm.es
[(5)] Professor (b), *Email:* s.franchini@upm.es

(a) Área Departamental Aeronáutica, Facultad de Ingeniería, Universidad Nacional de La Plata, La Plata, Buenos Aires, Argentina.

(b) IDR/UPM, E.T.S.I. Aeronáuticos, Universidad Politécnica de Madrid, E-28040, Madrid, Spain

ABSTRACT

The pararotor as decceleration system is a good candidate as an atmospheric probe for a planet with a dense enough atmosphere. The results summarized here are those obtained in some recent research projects concerning the aerodynamics modelization, the stability analysis and vertical wind tunnel tests. The stability study gives information relevant to the mass distribution allocation inside the probe, in order to obtain a stable flight. It is shown that the stability map can be defined in terms of the ratios of moments of inertia, but some variations can be found if the pararotor blades are asymmetrically tilted. Some experimental results obtained with almost free flying models in a vertical wind tunnel with the aim of validating the theoretical model, are reported as well.

1. INTRODUCTION

Research on the behaviour of rotating wing decelerators has been carried out for the last four years. The purpose of this research effort is to know the capabilities of this kind of device as an aerodynamic decelerator. The papers found in the literature related with the subject [1-11] did not offer relevant findings on the behavior of the type of pararotor considered here (featuring a low aspect ratio rotating wings). To our knowledge, the first two papers directly devoted to low aspect ratio rotating wings have been published recently: [12] deals with the stability of a free falling pararotor, and [13] with a semi-empirical model for the aerodynamic behaviour of a low aspect ratio pararotor in autorotation at low Reynolds numbers. This last one includes the presentation of an experimental study of a pararotor that rotates fixed to a shaft.
The studies presented here are the stability analysis of a free falling pararotor and the experimental investigation on small models that fly in a vertical wind tunnel. Finally, this theoretical model is analyzed related to the tests. Conclusions are drawn.

2. THEORETICAL MODEL. STABILITY STUDY

To elaborate this theoretical model the motion equations for an almost free falling pararotor have been formulated. These equations allow us to study motion stability. Motion stability depends on two nondimensional parameters (N_e and k_e, defined later on), which contain geometric, inertia and aerodynamic characteristics of the device. Based on these two parameters a stability diagram can be defined. Some stability regions (in the plane N_e,k_e) with different types of stability trajectories (nodes, spirals, focuses) can be identified for spinning motion around axes close to the major, minor and intermediate principal axes. It is found, for instance, that the aerodynamic forces acting on the blades contribute to the stability in the case of rotation around the intermediate principal inertia axis, which would be unstable in a vacuum. Then, the equations for determining the angles of nutation and spin of the body are shown, that define the orientation of the body for a steady motion. The parameters on which the orientation depends are also shown.

2.1 Rotational motion equations

As aforementioned, the system analyzed consists of a cylindrical body, with two identical blades that rotates at angular velocity $\overline{\omega}=(\omega_1, \omega_2, \omega_3)$, and falls vertically at uniform velocity U_∞. The geometry is defined in Fig. 1. The body-fixed reference system, 1,2,3, has its origin at the center of mass and directions e_1,e_2,e_3. The axes 1,2,3 are principal axes of the body. The inertial reference system is X,Y,Z; its axes have the directions i,j,k. The blades are located on the plane 1,2.
To simplify Euler´s equations the following assumptions have been considered: 1) the angles of attack, the angle of incidence of the blade and of the flow to the blades are all small; and 2) the component along the 1 axis of the relative velocity to the blade

does not have an aerodynamic influence. Also, the effect of the higher order terms has been neglected.
By using the aforementioned simplifying assumptions, the equations of rotational motion around the center of mass for the vertical free falling pararotor are

$$\dot{\omega}_1 - \frac{B-C}{A}\omega_2\omega_3 = -\frac{k_A^{-1}}{t_c^2}k_{21}\left(\delta_\beta - \frac{\omega_2}{\omega_3}\right) \quad (1a)$$

$$\dot{\omega}_2 + \frac{A-C}{B}\omega_1\omega_3 = \frac{k_B^{-1}}{t_c^2}\left(\delta_\beta - \frac{\omega_2}{\omega_3}\right) \quad (1b)$$

$$\dot{\omega}_3 - \frac{A-B}{C}\omega_1\omega_2 = \frac{1}{t_c^2}\left[\phi\alpha_0 + \frac{\omega_2}{\omega_3}\left(\frac{\omega_2}{\omega_3} - \delta_\beta\right) - \frac{c_D(\alpha_0)}{c_{L\alpha}}\right] \quad (1c)$$

where

$$\beta_1 = \beta_0 + \delta_\beta \;\; ; \;\; \beta_2 = \beta_0 - \delta_\beta \;\; ; \; \alpha_0 = \phi - \beta_0$$

$$k_A = \frac{A}{C} \; ; \; k_B = \frac{B}{C} \; ; \; k_{21} = \frac{r_{p12}}{r_{p11}} \; ; \quad t_c^2 = \frac{C}{c_{L\alpha} r_{p11} S\rho (r_{p11}\omega_0)^2} \quad (2)$$

A, B, C are the principal moments of inertia; c_D, is the drag coefficient of the blade; $c_{L\alpha}$,, is the slope of the curve lift vs. angle of attack for the blade; S is the area of one blade; r_{pij} is the component j of the vector position of the center of pressure of the blade i (j = 1, 2, 3; i = 1, 2); ρ is the atmosphere gas density; ω_0 is the angular velocity along the 3 axis; and ϕ is the angle of incidence of the flow to the blades.

2.2 Stability analysis

Eq. (1c) can be decoupled from the others. Then, the solution for the equilibrium is found to be

$$x_2 = x_{2e} = \delta_\beta N_e / \left(N_e - 1\right) \quad (3a)$$

$$x_1 = x_{1e} = -\frac{\delta_\beta}{k_{21}}\frac{C-B}{C-A}\frac{N_e}{1-N_e} \quad (3b)$$

where $x_1 = \omega_1/\omega_0$ and $x_2 = \omega_2/\omega_0$.
$N_e = I_a c_{L\alpha} k_{21} / \left(C - B\right)$ is called "the stability number". The stability of the equilibrium points is analyzed by following the classical perturbation method, through the characteristic equation of the autonomous system that defines the evolution of the trajectories of the system (either stable or unstable nodes, focuses or spirals) as a function of the values of the mentioned two parameters (N_e and k_e). This last is defined as:

$k_e = 4k_{21}{}^2 \frac{B}{A}\frac{C-A}{C-B}$, so-called "the ratio of the moments of inertia".

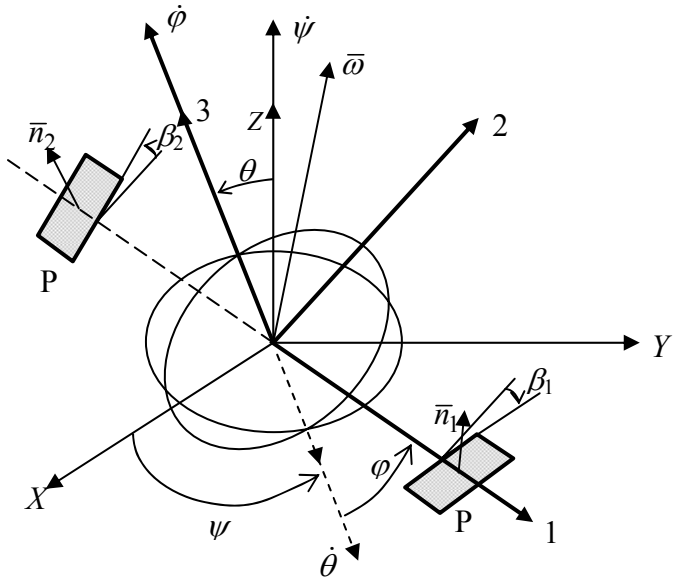

*Figure 1. System geometry. (X,Y,Z), inertial reference system; (*1,2,3*), body-fixed reference system; ψ, precession angle; θ, nutation angle; φ, spin angle;* $\overline{\omega}$ *, angular velocity*

2.3 Stability regions

As the signs of the differences of moments of inertia have an influence in the stability limits, their relative value should be taken into account. The results of this analysis can be displayed in a plane (N_e, k_e). These parameters define the stability regions. They are summarized in Table 1.

2.4 Determination of body attitude

The nutation angle, θ, and spin angle, φ, (Fig. 1) are determined from system equations for the components of the angular velocity $\overline{\omega}$ in the body-fixed axes, for stationary motion $\dot{\theta} = 0$ (see [12]).

It can be demonstrated [12] that $\overline{\omega}$ is a vector along the Z axis direction, as it is shown in Fig. 2.

Table 1. Stability cases

Case **Spinning motion close to:**	Relation of inertia moments	Stable regions
the major axis of inertia. Inertial stability	$A, B < C$	$0 < N_e < 1$, $k_e > 0$
the axis of lower inertia. Inertial stability*	$A, B > C$	$N_e < 0$, $k_e > 0$
the axis of intermediate inertia. Aerodynamic stabilization.	$B < C < A$	$N_e > 1$, $k_e < 0$
the axis of intermediate inertia. No stability.	$A < C < B$	No stability

* In a vacuum this case becomes unstable when internal energy dissipation is included

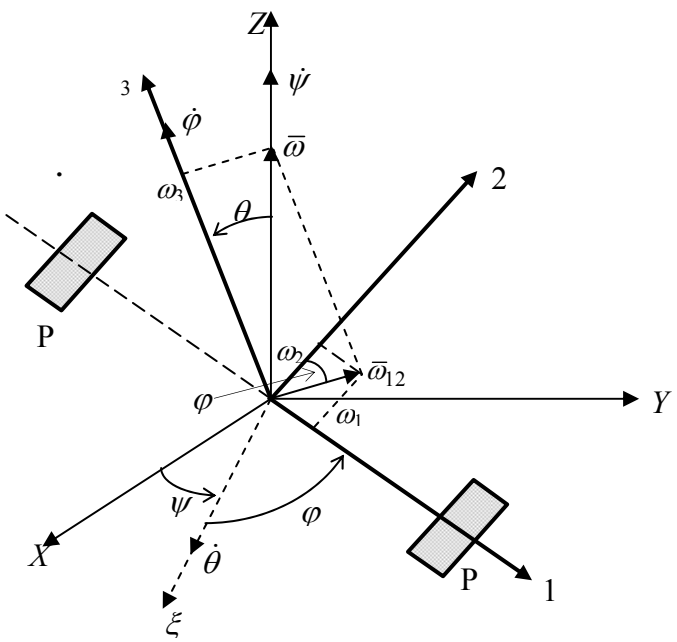

Figure 2. Orientation of the body. (X,Y,Z), inertial reference system; (1,2,3), body-fixed reference system; ψ, precession angle; θ, nutation angle; φ, spin angle. The angular velocity, $\bar{\omega}$, has the Z axis direction.

Then, it is found that the motion of the body is just pure precession ($\dot{\psi} \neq 0,\ \dot{\varphi} = \dot{\theta} = 0$) at a constant speed, given by $\dot{\psi} = \omega_3 / \cos\theta$; and that the spin angle is

$$\tan\varphi = \frac{\omega_1}{\omega_2} = \frac{1}{k_{21}} \frac{B - C}{A - C} \tag{4a}$$

where it is also seen that the spin angle is kept constant and depends only on the mass distribution and the position of the blades, and does not depend on δ_β. On the other hand, the nutation angle is

$$\tan\theta = -\left(\frac{N_e}{1 - N_e}\right) \frac{\delta_\beta}{|\cos\varphi|} \tag{4b}$$

It is deduced that, for small angles of nutation, the nutation angle is proportional to δ_β..
Eqs. (4) could also be used for the non-steady case (small motions around the equilibrium position) if $\dot{\theta}$ and $\dot{\varphi}$ are small enough.

3. VERTICAL WIND TUNNEL TESTS

3.1 Experimental Set Up

The experimental set up consists of a vertical wind tunnel (Fig. 3). A 5500 m^3/h fan is located at the lower part of the wind tunnel. The air discharges to a diffuser, through a straightener. The test section is a part of the diffuser. The diffuser shape has been so designed to attain vertical stability of the model. The diffuser has a constant depth of 0.28 m; bottom width 0.29 m, top width 0.57 m and length 2.25 m. The test section dimensions are: bottom width 0.29 m, top width 0,57 m and length 0.5 m.

3.2 Models description

The tested models consist of a hollow cylinder and two rectangular blades of bare aluminium alloy. Inside the cylinder there is a guide located at the center of mass, to allow the model to move along the guiding wire. Two sets of cylinders and three sets of blades have been used for the present analysis (Fig. 4). The combination of sets of blades and cylinders gives different relations of principal moments of inertia of the complete model. The other dimensions of the tested models are shown in Tables 2 and 3.

Table 2. Tested cylinders heights

Configuration	*h*, mm
*C*05	26
*C*06	56

Table 3. Tested blades thicknesses

Configuration	*e*, mm
*P*01	0.5
*P*02	0.8
*P*03	0.3

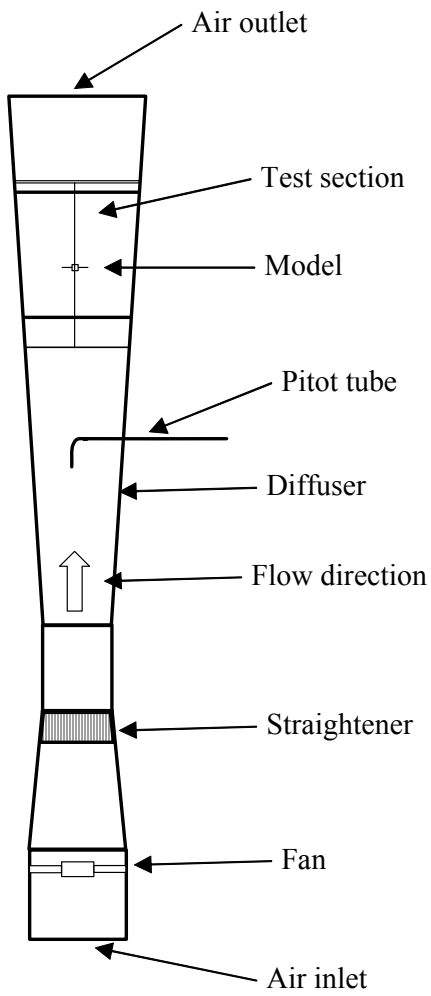

Figure 3. Sketch of the experimental set up. Vertical wind tunnel.

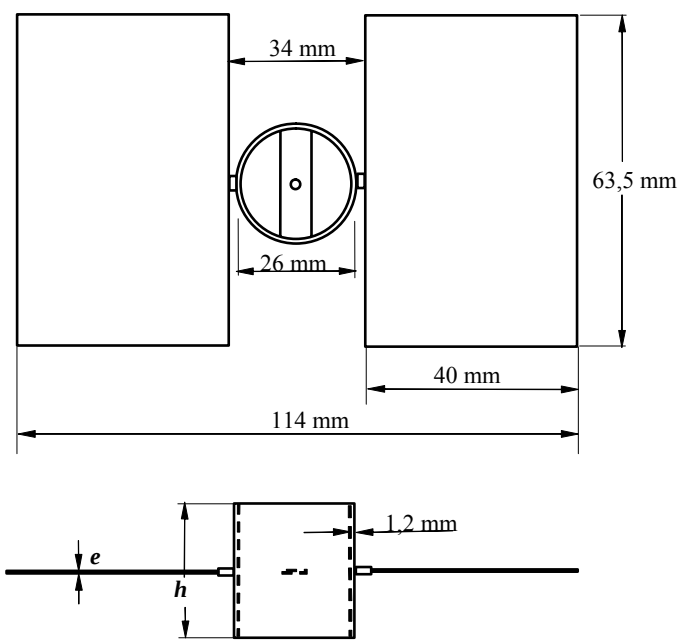

Figure 4. Model dimensions.

As aforementioned, a given model is the result of a specified combination of a cylinder and a set of blades. In Table 4, the masses and inertia moments of the tested models are presented.

Table 4. Tested model weight and inertia moments

Configuration	Mass [g]	A x 10^6 [kg m^2]	B x 10^6 [kg m^2]	C x 10^6 [kg m^2]
*C*05*P*01	15.2	3.5	8.9	11.6
*C*05*P*02	20.1	5.4	21.2	25.9
*C*05*P*03	11.6	1.9	5.8	6.9
*C*06*P*02	28.1	9.5	25.3	27.1
*C*06*P*03	19.6	5.9	9.8	8.1
*C*05*P*02*M*01	22.7	10.1	22.5	31.8

The model *C*05*P*02*M*01 has two 2.2 g masses located at body axes coordinates (mm): (17,–32,0) and (–17,32,0). The original purpose of introducing these masses has been to allow for variations of the inertia moment ratios.

3.3 Definitions, measured parameters and instrumentation

The following parameters have been measured: the spin velocity, measured by means of a stroboscopic lamp (resolution 50 rpm); the blade pitch angle, with a goniometer (resolution 1 deg); the flow velocity by a standard pitot-tube NPL type and a micromanometer (resolution 0.5 Pa); and the model weight, by means of a balance (resolution 0.01 g).
There are two additional interesting parameters: the angle of the mean plane between the blades $\delta_\beta = (\beta_1 - \beta_2)/2$ and the difference of pitch angle between the blades $\varepsilon = \beta_1 + \beta_2 = 2\beta_0$.

3.4 Tests

Several tests have been performed on the models described in Table 4, for the blades pitch angles shown in Tables 5 and 6, where the mean values of the parameters k (tip velocity ratio) and C_{DM} (equivalent pararotor drag coefficient) are also shown. N indicates the number of tests performed.
Photographs and videos with and without stroboscopic illumination have also been taken in order to study the body attitude.

3.5 Results and discussion on the experiments

Results concerning the velocity ratio k and the drag coefficient C_{DM} are shown in Figs. 5 and 6. From these tests, it can be seen that:
1) For the configurations with equal value of the pitch angle of both blades (–2, –4, –6, and –8 deg.), both the velocity ratio k and the drag coefficient of the model C_{DM} decrease as the blades pitch angle increases.

Table 5. Tests performed for configuration *C*05P02

β_1 deg	β_2 deg	δ_β deg	ε deg	k	C_{DM}	N
–12	8	–10	–4	0.39	3.06	1
–12	10	–11	–2	0.46	3.38	1
–10	–10	0	–20	–	–	1
–10	4	–7	–6	0.32	3.30	1
–10	6	–8	–4	0.36	3.25	2
–10	8	–9	–2	0.43	3.38	1
–8	–8	0	–16	0.21	2.99	3
–8	–8	0	–16	0.32	2.13	1
–8	–4	–2	–12	0.22	3.24	3
–8	0	–4	–8	0.24	3.39	3
–8	2	–5	–6	0.34	3.41	2
–8	4	–6	–4	0.37	3.48	3
–8	6	–7	–2	0.40	3.61	2
–8	10	–9	2	0.49	3.19	1
–6	–8	1	–14	0.25	2.41	1
–6	–6	0	–12	0.24	3.18	4
–6	2	–4	–4	0.38	3.36	1
–6	4	–5	–2	0.45	3.40	2
–4	–8	2	–12	0.25	2.85	1
–4	–6	1	–10	0.26	3.01	1
–4	–4	0	–8	0.26	3.24	6
–2	–2	0	–4	0.27	3.44	3

Table 6. Tests performed for the other configurations*

Configuration	β_1,deg	β_2,deg	δ_β,deg	ε,deg	k	C_{DM}
*C*05*P*03	–12	10	–11	–2	0.39	3.33
*C*05*P*03	–10	8	–9	–2	0.36	3.49
*C*05*P*03	–6	–6	0	–12	0.24	3.06
*C*05*P*03	–6	0	–3	–6	0.30	3.67
*C*05*P*03	–4	–6	1	–10	0.25	3.33
*C*05*P*03	–4	–4	0	–8	0.30	3.38
*C*05*P*01	–12	10	–11	–2	0.44	3.32
*C*05*P*02*M*01	–8	–8	0	–16	0.25	2.51
*C*05*P*02*M*01	–6	–6	0	–12	0.27	2.62
*C*05*P*02*M*01	–4	–4	0	–8	0.31	2.81
*C*05*P*02*M*01	–2	–2	0	–4	0.38	3.03
*C*06*P*02	–8	–8	0	–16	0.32	2.13
*C*06*P*02	–6	–6	0	–12	0.24	2.30
*C*06*P*02	–4	–4	0	–8	0.27	2.30
*C*06*P*02	–2	–2	0	–4	0.31	2.54
*C*06*P*03	–6	–6	0	–12	–	–
*C*06*P*03	–4	–4	0	–8	–	–
*C*06*P*03	–2	–2	0	–4	–	–

**N*=1

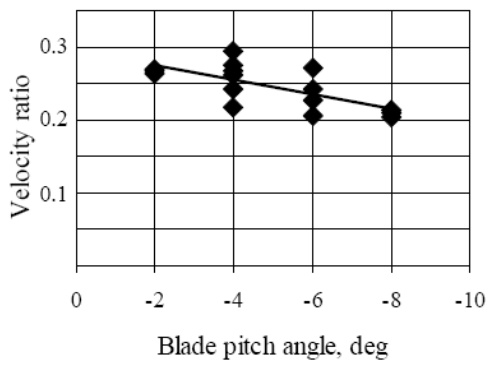

Figure 5. Configuration C05P02. Velocity ratio vs. blade pitch angle.

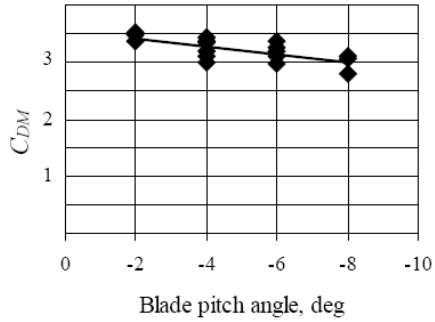

Figure 6. Configuration C05P02. Model drag coefficient vs. blade pitch angle.

2) Related to the value of the angle between blades ε it can be seen, as expected, that k decreases as $|\varepsilon|$ increases (the model spins faster). On the other hand C_{DM} increases as $|\varepsilon|$ decreases.
3) Concerning the angle of the mean plane between the blades δ_β, k decreases as δ_β decreases.

A regards attitude and stability of the model, it is shown that:
1) As the theoretical model predicts, the tested models have shown stable motion when *C*>*A*,*B* and unstable motion when *B*>*C*>*A*. This feature is described below.
2) For the configurations with one blade at positive pitch angle and the other at negative, it has been observed that the model rotates close to an axis perpendicular to the mean plane between the blades (Fig. 7). As is shown in Fig. 7, the cylinder is tilted, and then its symmetry axis rotates around the vertical direction (*Z* axis). The inclination of the cylinder symmetry axis increases as the mean plane between blades δ_β increases and the difference of pitch angle between blades ε decreases (for *C*05*P*02, β_1 = –12°, β_2 = 10°, ε = –2° the cylinder shows the maximum inclination among the configurations tested).

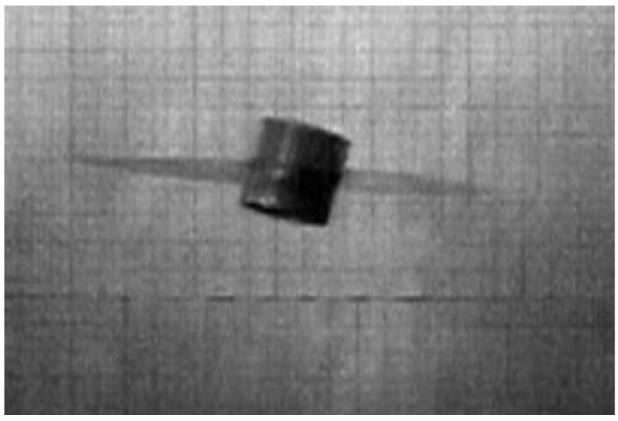

Figure 7. Attitude of the model C05P02 for β_1 = –12°, β_2 = 10°, ε = –2°.

As the inertia moment of the blades diminishes, the body rotates around an axis closer to the cylinder

symmetry axis (*C*05*P*03, *C*05*P*01) for the same blade pitch angles tested.
3) For the configuration *C*05*P*03, β_1 = -12°, β_2 = 10° and β_1 = -10°, β_2 = 8°, an oscillation of the model around the body axis 1 (Fig. 8) has been observed.
4) During the tests the inclination of the model rotation axis (body axis 3) changed with time in an unpredictable way. The attitude of the models varies slowly, the rotation axis showing a small, almost constant nutation motion (Fig. 9).

(Figs. 8 and 9 placed at the end).

4. THEORETICAL MODEL VALIDATION

From the vertical wind tunnel tests it is shown that:
1) The models and configurations tested have exhibited stable motions when *C>A,B* (Fig. 11) and unstable motions when *B>C>A* (Fig. 12) in agreement with the theoretical model predictions.

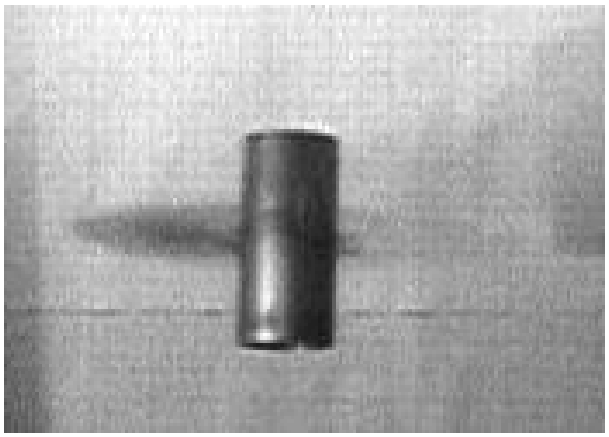

Figure. 10. Attitude of the model C06P02 for β_1 =–4°, β_2 = –4°. C>B>A. Stable motion.

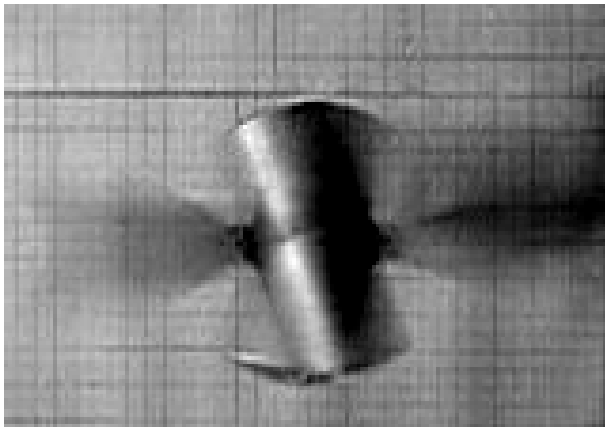

Figure. 11. Attitude of the model C06P03 for β_1 = –4 °, β_2 = –4°. B>C>A. Unstable motion.

2) In the cases described in Section 3 where the cylinder symmetry axis is not perpendicular to the blade mean plane $\delta_\beta \neq 0$, the body axis 3 does not coincide with that symmetry axis, and there is a small angle with the perpendicular to the mean plane between the blades. The theoretical model predicts that the body axis 3 should have an inclination with regard to the vertical direction $\overline{\omega}$, but small (less than 1°) for the tested models, and, therefore, difficult to measure.

5. CONCLUSIONS

5.1 Concerning the experiments

1) It has been found that the models hover following either stable or unstable patterns, according to the ratio of moments of inertia, as predicted by the theoretical stability model.
2) Both the velocity ratio *k* and the drag coefficient of the model C_{DM} decrease as the blades pitch angle increases.

5.2 Concerning the analysis relating the experiments and the theoretical model

1) The theoretical model correctly predicts the instability for a pararotor with the relation of principal inertia moments *B>C>A*. It was not possible to measure the inclination of the body axis in the vertical wind tunnel tests, to compare it with the predictions of the theoretical model, because the nutation angle for the tested configurations is small.

5.3 Concerning pararotors as aerodynamic decelerators

1) The pararotor is a viable concept as an aerodynamic decelerator.
2) The behaviour of devices with low-aspect-ratio wings has been studied both experimentally and theoretically. The parameters, which determines the behaviour of the pararotor and the magnitude of their influence, are known in such a way that a specific application could be followed.

6. REFERENCES

1. Crimi, P., “Analysis of samara-wing decelerator steady-state characteristics”, *Journal of Aircraft*, Vol. 25, No. 1, 1988, pp. 41-47.
2. Karlsen, L., Borgström, D. and Paulsson, L., “Aerodynamics of a rotating body descending from the separation position of an artillery munition shell”, AIAA-91-0870-CP, April 1991.
3. Pepper Jr, W., “A new rotating parachute design having high performance”, *Journal of Spacecraft and Rockets*, Vol. 23, No. 2, 1986, pp. 222-224.
4. Shpund, Z. and Levin, D., “Measurement of the static and dynamic coefficients of a cross-type

parachute in subsonic flow", AIAA paper 91-0871-CP, April 1991.
5. Levin, D. and Shpund, Z., "Dynamic investigation of the angular motion of a rotating body-parachute system", *Journal of Aircraft*, Vol. 32, No. 1, 1995, pp. 93-99.
6. Shpund, Z. and Levin, D., "Forebody influence on rotating parachute aerodynamic properties", *Journal of Aircraft*, Vol. 34, No. 2, 1997, pp. 181-186.
7. Levin, D. and Shpund, Z., "Canopy geometry effect on the aerodynamic behaviour of cross-type parachutes", *Journal of Aircraft*, Vol. 34, No. 5, 1997, pp. 648-652.
8. Rosen, A. and Seter, D., "Vertical autorotation of a single winged samara", *Journal of Applied Mechanics*, Vol. 58, No. 4, Dec. 1991, pp. 1064-1070.
9. Seter, D. and Rosen, A., "Stability of the vertical autorotation of a single winged samara", *Journal of Applied Mechanics*, Vol. 59, No. 4, Dec. 1992, pp. 1000-1008.
10. Stahl, W. H., "Aerodynamics of low aspect ratio wings", Missile aerodynamics, *AGARD Lecture Series*, No. 98, , 1979, pp. 1-64.
11. Pelletier, A. and Mueller, T. J., "Low Reynolds Number Aerodynamics of Low-Aspect-Ratio, Thin/Flat/ Cambered -Plate Wings", *Journal of Aircraft*, Vol. 37, No. 5, 2000, pp. 825-832.
12. Nadal Mora, V. and Sanz Andrés, A., "Stability Analysis of a Free Falling Pararotor", *Journal of Aircraf,* Vol. 43, No. 4, 2006, pp. 980-986.
13. Nadal Mora, V., Sanz Andrés, A. and Cuerva, A. "Model of the aerodynamic behavior of a pararotor", *Journal of Aircraf,* Vol. 43, No. 6, 2006, pp. 1893-1903.
14. Nadal Mora, V., "Comportamiento aerodinámico de sondas atmosféricas en entornos aeroportuarios", *Tesis doctoral*, Universidad Politécnica de Madrid, España, May 2005.

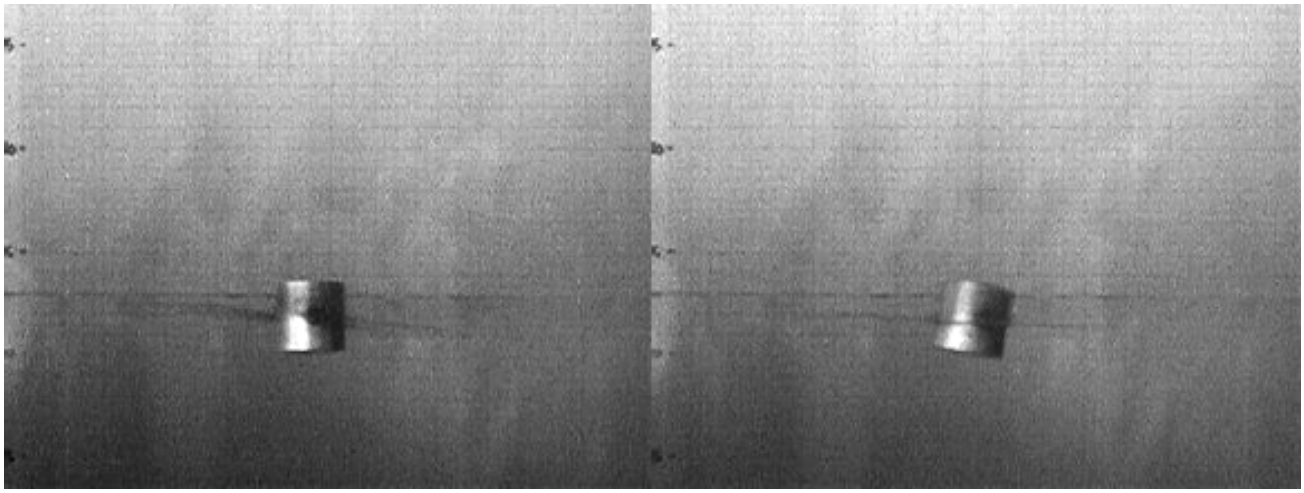

Figure. 9. Attitude of the model C05P03 for $\beta 1 = -12°$, $\beta 2 = 10°$, $\varepsilon = -2°$.

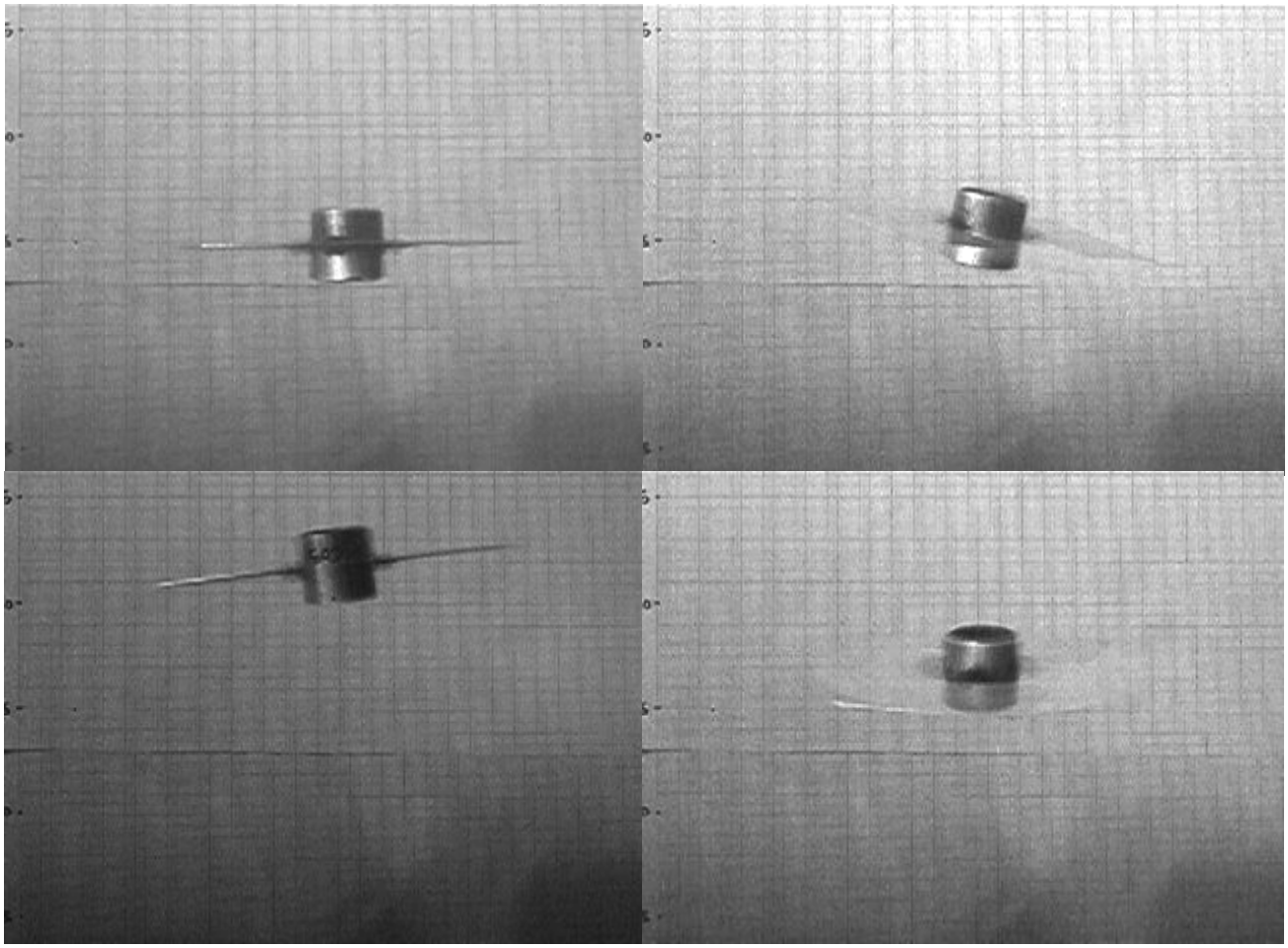

Figure. 10. Attitude of the model C05P02 for $\beta_1 = -6°$, $\beta_2 = 4°$.